Springer

KSME

Journal of Mechanical Science and Technology 26 (2) (2012) 437~446
www.springerlink.com/content/1738-494x
DOI 10.1007/s12206-011-1208-z

Unsteady flow field numerical calculations of a ship's rotating Weis-Fogh-type propulsion mechanism with the advanced vortex method †

Ki-Deok Ro[1,*], Baoshan Zhu[2] and Michihisa Tsutahara[3]

[1]*Department of Mechanical system Engineering · Institute of Marine Industry, Gyeonsang National University, Gyeongnam 650-160, Korea*
[2]*Department of Thermal Engineering, State Key Laboratory of Hydroscience and Engineering, Tsinghua University, 100084 China*
[3]*Department of Mechanical Engineering, Kobe University, 657-8501 Japan*

(Manuscript Received February 4, 2011; Revised August 31, 2011; Accepted October 3, 2011)

Abstract

The Weis-Fogh mechanism, found in the hovering flight of a small bee, is a unique and efficient lift generation. In this study, we proposed a rotating type propulsion model that applies the principle of the Weis-Fogh mechanism and calculated the unsteady flow field of the propulsion model with the advanced vortex method. The wing (NACA0010 airfoil) and channel are approximated by source and vortex panels, and free vortices are introduced away from the body surfaces. The viscous diffusion of fluid is represented using the core-spreading model to the discrete vortices. We investigated the thrust and drag coefficients, pressure field, vorticity field, velocity vector field, and average propulsive efficiency of the propulsion model by changing the rotating angle velocity. The force acting on the wing depended heavily on the directions of the thrust and drag and the thrust and drag coefficients largely fluctuated with the change in the rotating angles. The average thrust increased as the rotating angle velocity increased. The maximum propulsive efficiency was 27.9% at a calculated angle velocity. The flow field of this rotating type propulsion mechanism is unsteady and very complex because the wing rotates and moves unsteadily in the channel. However, using the advanced vortex method, it could be calculated accurately.

Keywords: Computational fluid dynamics; Vortex method; Propulsion mechanism; Unsteady flow; Rotating wing

1. Introduction

The Weis-Fogh mechanism [1, 2] was discovered by observing the hovering flight of a small bee called Encarsia formosa. Its higher efficiency and unique lift generation mechanism are attracting much attention [3-7]. Vigorous attempts have been made to make use of this mechanism for engineering applications [8-17]. The studies for applying the mechanism to a ship's propulsion mechanism are as follows.

Tsutahara et al. [9] proposed a propulsion model that was characterized by a two dimensional model of the mechanism using a pair of flat-plate wings installed in a water channel. These researchers demonstrated that the propulsion model effectively works as a ship's propulsion mechanism through experiments measuring thrust and drag. Ro et al. [13] used an advanced vortex method to simulate unsteady velocity and pressure fields generated around the wing when the propulsion mechanism is in operation, and calculated the time variation of thrust and drag acting on the wing. Furthermore, in hopes of developing practical applications of this propulsion mechanism, Ro et al. recently improved the propulsive efficiency by using rubber-type [14] and spring-type [15] elastic wings, executing a sailing test of a model ship [16] and fluctuation characteristics tests [17] on a variety of propulsion models to realize the possibility of practical applications of this mechanism.

Because most of the currently used power generating mechanisms are rotating types and the propulsion mechanism mentioned above is a reciprocating one, mechanical loss is unavoidable during the conversion of rotating motion to reciprocating motion. Therefore, in this study, we proposed a ship's propulsion model of a rotating type that uses Weis-Fogh mechanism, which has similar motion to the reciprocating type.

The unsteady flow fields for the Rotating Weis-Fogh-type propulsion mechanism are verified by using an advanced vortex method [13, 18]. The vortex methods [19] consist of a simple algorithm based on the physics of flow, and provide easy-to-handle and completely grid-free Lagrangian calculations of unsteady and vortical flows without the use of any Reynold's averaged Navier-Stokes (RANS) type turbulence models. The methods are also utilized to devise an advanced scheme of simulating the unsteady viscous flow through a rotating Weis-Fogh type ship propulsion mechanism.

† This paper was recommended for publication in revised form by Associate Editor Man-Yeong Ha

* Corresponding author. Tel.: +82 55 772 9103, Fax.: +82 55 772 9109
E-mail address: rokid@gnu.ac.kr

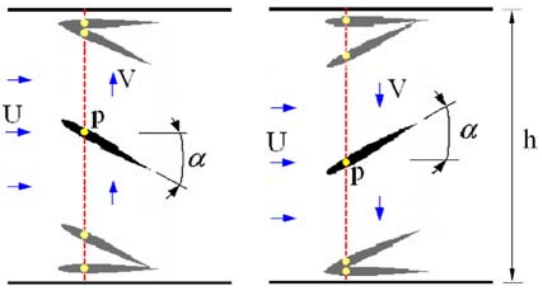

(a) Reciprocating type

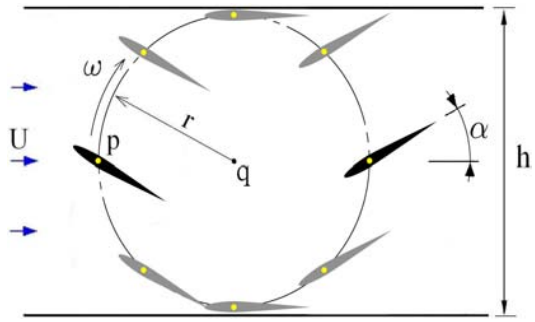

(b) Rotating type

Fig. 1. Models of the Weis-Fogh type propulsion mechanism.

2. Calculation method

2.1 Reciprocating and rotating type propulsion models

Fig. 1 shows (a) the reciprocating type and (b) the rotating type propulsion models of the Weis-Fogh mechanism. In the reciprocating type propulsion model, when point p that corresponds to the center pivot point of the wing oscillates perpendicular to the uniform flow U at the velocity V, the wing first opens from the lower wall, then moves translationally maintaining the opening angle of α, and finally rotates and closes on the upper wall. Then, the wing repeats the motion: it rotates and opens from the upper wall, moves translationally, and finally rotates and closes on the lower wall. This wing movement generates thrust on the left side of the figure, that is, in the opposite direction of the uniform flow U. In the rotating type propulsion model, point p rotates counterclockwise at angular velocity ω, maintaining the rotation radius r in the center of the water channel in which the uniform flow U flows. At this point, the trailing edge of the wing is touching the lower wall, and it rotates and opens with the pivot point as its center (opening stage). Then, maintaining the opening angle α, it moves upward (translating stage) and closes with the leading edge touching the upper wall (closing stage). The wing repeats this motion: it rotates and opens from the upper wall, moves downward, and finally rotates and closes on the lower wall. This wing movement is almost similar to the movement demonstrated by the reciprocating type. Thrust is generated in the opposite direction of the uniform flow, which is the direction of the progress of the ship.

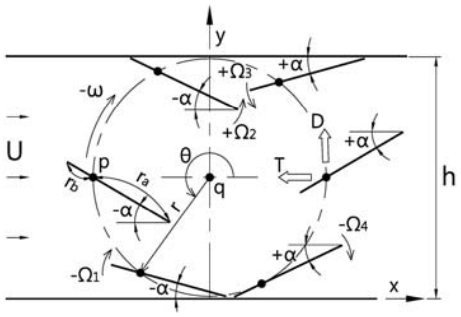

Fig. 2. An analytical model of rotating type.

2.2 Calculation of the position and velocity of the wing

Fig. 2 shows an analytical model of a rotating type Weis-Fogh propulsion mechanism. In the actual calculation, a NACA0010 type wing was used as in the previous calculation of the reciprocating movement [13], but in the analytical model of Fig. 2, it was represented by a flat-plate wing equivalent to the chord of the wing in order to simplify the calculation method. Point p on the wing shift rotates counterclockwise with angular velocity ω, maintaining its rotation radius r and its center at point q. We used orthogonal coordinates for the calculations. We aligned the lower wall of the water channel with the x-axis, and the axis that is perpendicular to the uniform flow U and passes through point q (the rotating center) was aligned to the y-axis. The coordinates of point p, (x_p, y_p), at the random rotating angle θ, can be easily calculated as

$$x_p = r\cos\theta + x_q \tag{1a}$$

$$y_p = r\sin\theta + y_q\,. \tag{1b}$$

Here, (x_q, y_q) is the coordinates of the rotating center. In the calculation, the starting point p on the wing shaft was set as the origin of the orthogonal coordinates. Therefore, the rotating angle θ at the n-th time step can be calculated as $\theta = 3\pi/2 - \omega\, n\, dt$, when the time step is dt.

In the first opening stage of Fig. 2, the wing rotates around point q keeping the radius r from point p to rotation center q constant. At the same time, the wing itself rotates around the point p, and keeps its trailing edge touching the wall in order to open. The rotating angular velocity Ω_1 around point p at the this stage can be calculated based on the geometric relations

$$r - r\cos(3\pi/2 - \theta) = r + r\sin\theta \tag{2a}$$

$$r_\alpha \sin\alpha = r + r\sin\theta\,. \tag{2b}$$

If we define $\Omega_1 = d\alpha/dt$, and $\omega = d\theta/dt$, we can obtain from Eq. (2b),

$$r_\alpha \cos\alpha\, \Omega_1 = r\cos\theta\,\omega \tag{2c}$$

$$\therefore\ \Omega_1 = \frac{r\cos\theta\omega}{r_a\cos\alpha}. \tag{2d}$$

Similarly, the rotating angular velocity Ω_2 around point p at the first closing stage and the rotating angular velocities Ω_3 and Ω_4 at the second opening and closing stages, respectively, are calculated as follows:

$$\Omega_2 = -\frac{r\cos\theta\omega}{r_b\cos\alpha} \tag{3}$$

$$\Omega_3 = -\frac{r\cos\theta\omega}{r_a\cos\alpha} \tag{4}$$

$$\Omega_4 = \frac{r\cos\theta\omega}{r_b\cos\alpha}. \tag{5}$$

Here, r_a and r_b represent the distance from the trailing and leading edges of the wing to point p, respectively, and α represents the opening angle of the wing at each time step. We should note that as shown in Fig. 2, the rotating angle velocities ω and Ω (Ω_1~Ω_4) are negative (-) when they move clockwise and positive (+) when they move counterclockwise with the rotating axis as the center. The opening angle α is the angle between the x-axis and the wing chord at the trailing edge, and from the x-axis, clockwise is calculated as negative (-) and counterclockwise as positive (+). In the translating stages, the rotating angular velocity $\Omega = 0$.

If the coordinates of the trailing edge are (x_t, y_t), the coordinates of a random point (x_A, y_A) on the airfoil wing surface are

$$x_A = r_x\cos\alpha - r_y\sin a + x_t \tag{6a}$$

$$y_A = r_x\sin\alpha - r_y\cos\alpha + y_t. \tag{6b}$$

Here, r_x and r_y are $r_x = (x_A - x_t)$, $r_y = (y_A - y_t)$. Based on the resolution of the wing's movement, we can calculate the velocities υ_{Ax} and υ_{Ay} in the x and y directions at a random point (x_A, y_A) of the wing surface and the tangential and normal velocities $\mathbf{v_A}\cdot\tau$ and $\mathbf{v_A}\cdot\mathbf{n}$ as follows:

$$\begin{aligned}\mathbf{v_A} = \upsilon_{Ax}\mathbf{i} + \upsilon_{Ay}\mathbf{j} &= \left[\left(x_A - x_q\right)\mathbf{i} + \left(y_A - y_q\right)\mathbf{j}\right]\times\omega\mathbf{k} \\ &+\left[\left(x_A - x_P\right)\mathbf{i} + \left(y_A - y_P\right)\mathbf{j}\right]\times\Omega\mathbf{k} \\ &= \left[\omega\left(y_A - y_q\right) + \Omega\left(y_A - y_q\right)\right]\mathbf{i} \\ &-\left[\omega\left(x_A - x_q\right) + \Omega\left(x_A - x_P\right)\right]\mathbf{j}\end{aligned} \tag{7a}$$

$$\therefore\ \upsilon_{Ax} = \left[\omega\left(y_A - y_q\right) + \Omega\left(y_A - y_q\right)\right] \tag{7b}$$

$$\upsilon_{Ay} = -\left[\omega\left(x_A - x_q\right) + \Omega\left(x_A - x_P\right)\right] \tag{7c}$$

$$\mathbf{v_A}\cdot\boldsymbol{\tau} = \upsilon_{Ax}\cdot\tau_x + \upsilon_{Ay}\cdot\tau_y \tag{8a}$$

$$\mathbf{v_A}\cdot\mathbf{n} = \upsilon_{Ax}\cdot n_x + \upsilon_{Ay}\cdot n_y. \tag{8b}$$

Here, $\boldsymbol{\tau}$ and $\mathbf{n}$ are unit vectors in the tangential and normal directions, respectively, and $\mathbf{i}$, $\mathbf{j}$, and $\mathbf{k}$ are unit vectors in the x, y, and z directions, respectively. Also, (x_p, y_p) and (x_q, y_q) are the coordinates on the p and q axes in Fig. 2, respectively, and Ω and ω are the rotating angular velocities around each axis.

2.3 Calculation of the flow fields by the advanced vortex method

2.3.1 Introduction of a nascent vortex elements

By calculating the velocity and the pressure fields of this propulsion unit during the movement of the wing shown in Fig. 1(b) and Fig. 2 for every time step, we can predict the thrust and drag of the unit. As shown in Fig. 1(b), three objects -the wing, two plates of the channel- are present in the flow field. Two kinds of panels, source panels and vortex panels, are distributed on the surfaces of each object. A vortex panel resembles a vortex sheet with the vorticity distributed along the solid boundary of the object. At this time, the unknowns that should be determined at each time step are the source strength on the panel for M pieces and the circulation around the wing and two plates of the water channel. These unknowns are obtained using the Neumann condition in Eq. (9) at the center of the source panel for M pieces $(i = 1, 2, 3, \cdots, M)$, and the theorem of Kelvin in Eq. (10) for the circulation of each object perimeter, $\Gamma_b = \gamma_{bs}\cdot S_b$.

$$\left\{\sum_{j=1}^{M}(\boldsymbol{u}^{sp} + \boldsymbol{u}^{vp})_{ij} + \sum_{k=1}^{N}\boldsymbol{u}_{ik}^{vo} + U\right\}\cdot\boldsymbol{n}_i = \boldsymbol{u}_i\cdot\boldsymbol{n}_i \tag{9}$$

$$\Gamma_b + \sum_{k=1}^{N_b}\Gamma_{bk}^{vo} = 0 \tag{10}$$

Here, $\boldsymbol{u}^{sp}$, $\boldsymbol{u}^{vp}$ and $\boldsymbol{u}^{vo}$ are the induced velocities deduced from the source panels, the vortex panels, and the vortex elements introduced into the flow field; U and $\boldsymbol{u}_i$ are the uniform flow and the velocity of the i-th control point; $\boldsymbol{n}_i$ is the unit normal vector at the i-th point; γ_{bs} represents the circulation per unit length for each object along the perimeter S_b; and Γ_{bk}^{vo} is the circulation of the vortex element that is emitted by each object. Here, assuming that γ_{bs} is uniformly distributed around the object, it can be obtained from $\gamma_{bs} = \Gamma_b / S_b$, then $\boldsymbol{u}^{vp}$ is calculated by γ_{bs}. In the case of the conventional vortex method, this situation was found to be numerically unstable. In this paper, however, by considering a double fold of the source and vortex panels, the above unstable numerical problem could be eliminated.

Fig. 3 illustrates the schematic of the thin vorticity layer and the introduction of the nascent vortex elements. The vorticity field near the solid surface is represented by the proper distribution of the vorticity layers and the discrete vortex elements to satisfy the nonslip condition on the body surface. A thin vorticity layer with thickness h_i is considered along the body surface, and the solid body is discretized using source panels, as shown in Fig. 3. Assuming that the flow is two dimensional and that there is a linear distribution of the velocity in the thin vorticity layer, and for the simplicity of illustration, suppose

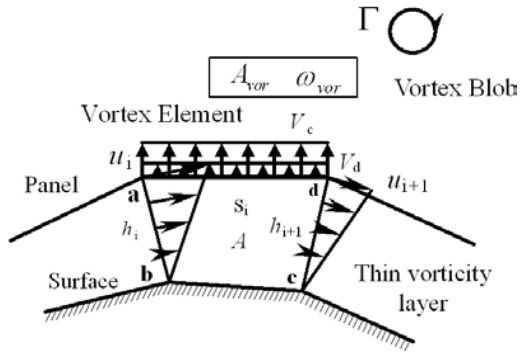

Fig. 3. Thin vorticity layer and nascent vortex element.

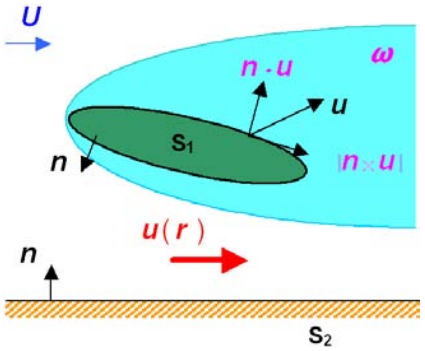

Fig. 4. Flow field involving vorticity region.

the body is stationary, the normal convective velocity V_c on the outer boundary of the vorticity layer can be expressed using the relation of continuity of flow and the no-slip condition on the body surface for the element of the vorticity layer [abcd] as

$$V_c = \frac{1}{s_i}\left\{\frac{h_i u_i}{2} - \frac{h_{i+1}u_{i+1}}{2}\right\} \tag{11}$$

in which s_i, h_i, and u_i represent the panel length, the thickness of the vorticity layer, and the tangential velocity at the panel edge. As the body is movable, Eq. (11) is still valid when u_i is a velocity relative to the moving body.

On the other hand, the vorticity of the thin shear layer diffuses through the panel into the flow field. In order to account for this vorticity diffusion, a diffusion velocity was employed in the same manner as the vorticity layer spreading method proposed by Kamemoto [18]. The vorticity layer spreading method is based on the viscous diffusion of the vorticity in the shear layer developing over a suddenly accelerated plate wall. In this case, the displacement thickness of the vorticity layer (δ) diffuses over time as $\delta = 1.136(\nu t)^{0.5}$ from the solid surface at time t. Differentiating δ by t and substituting the thickness of the vorticity layer h_i into δ, we obtain the diffusion velocity V_d at the outer boundary of the vorticity layer as

$$V_d = \frac{1.136^2 \nu}{h_i + h_{i+1}}. \tag{12}$$

Here, ν is the kinematic viscosity of the fluid. If the value of $(V_c + V_d)$ becomes positive, a nascent vortex element is introduced in the flow field, where the thickness h_{vor} and the vorticity ω_{vor} of the vortex element are obtained as follows:

$$h_{vor} = (V_c + V_d)dt \tag{13}$$

and,

$$\omega_{vor} = \frac{\Gamma}{A + A_{vor}}. \tag{14}$$

Here, Γ is the circulation originally involved in the element of the vorticity layer [abcd] calculated according to Eqs. (9) and (10), and A and A_{vor} are the areas of the vorticity layer element and the nascent vortex element. A vortex blob at fixed height is substituted for the square-type vortex element generated during each time step. Moreover, as a linear distribution of velocity is assumed in the thin vorticity layer, the shearing stress on the wall surface τ_w is approximated from the following equation, as long as the thickness of the vorticity layer is sufficiently thin:

$$\tau_w = \mu\frac{\partial u}{\partial y} = -\mu\omega. \tag{15}$$

2.3.2 Calculation of the velocity field

A trajectory of the vortex shedding element over the time step dt is approximated by applying the Adams-Bashforth method as

$$\boldsymbol{r}(t+dt) = \boldsymbol{r}(t) + \{1.5\boldsymbol{u}(t) - 0.5\boldsymbol{u}(t-dt)\}dt \tag{16}$$

in which the motion $\boldsymbol{u}$ of the vortex element can be derived from the following Biot-Savart law, Eq. (17), that includes source panels, vortex sheet panels, and all vortex elements existing in the flow field.

$$\boldsymbol{u}(\boldsymbol{r}) = \frac{1}{2\pi}\int_V \frac{\boldsymbol{\omega}\times\boldsymbol{R}}{R^2}dV - \frac{1}{2\pi}\times \int_{S_0}\left[\frac{(\boldsymbol{n}_0\cdot\boldsymbol{u}_0)\cdot\boldsymbol{R}_0}{R_0^2} - \frac{(\boldsymbol{n}_0\times\boldsymbol{u}_0)\times\boldsymbol{R}_0}{R_0^2}\right]dS_0 \tag{17}$$

$\boldsymbol{R}_0$ of the second term on the RHS of Eq. (17) represents $\boldsymbol{R}_0 = \boldsymbol{r} - \boldsymbol{r}_0$ and $R_0 = |\boldsymbol{R}_0|$. Moreover, the dot product $\boldsymbol{n}_0\cdot\boldsymbol{u}_0$ and the cross product $\boldsymbol{n}_0\times\boldsymbol{u}_0$ show the velocity components of the normal and tangential directions on the boundary surface, respectively, and they coincide with the source and the vortex distributions on the surface. Accordingly, as shown in Eq. (17) and Fig. 4, a velocity field of the viscous and incompressible flows corresponds to the field integration relating to the vorticity distributions in the flow field, the surface integra

tion concerning the source, and the vortex distribution around the boundary surface.

The Lagrangian expression for the vorticity transport equation is expressed as

$$\frac{d\boldsymbol{\omega}}{dt} = (\boldsymbol{\omega} \cdot grad)\boldsymbol{u} + \nu\nabla^2\boldsymbol{\omega} . \tag{18}$$

The first term of the RHS disappears for a two-dimensional case. The second term or the viscous diffusion term is approximated using the core spreading method [19].

$$\varepsilon_k(t+dt) = \varepsilon_k(t) + \frac{2.242^2\nu}{2\varepsilon_k(t)}dt \tag{19}$$

Here, ε_k is the core radio for k - th vortex element.

2.3.3 Calculation of the pressure field

If the divergence is applied to the Navier-Stokes equation, the pressure Poisson equation becomes

$$\nabla^2 p = -\rho div(\boldsymbol{u} \cdot grad\boldsymbol{u}) . \tag{20}$$

In general, the pressure field is obtained by calculating the Poisson equation using the finite difference method. However, in the process some lattices must be generated in the flow field which negates the advantages of the vortex method, i.e., no need for grid. Therefore, in this research, instead of using the finite difference method of the Poisson equation, the pressure in the flow field is obtained from the integration equation formulated by Uhlman [20] as follows:

$$\begin{aligned} &\beta H + \int_{S_0} H\frac{\partial G}{\partial \boldsymbol{n}}dS_0 = -\int_V \nabla(\boldsymbol{u}\times\boldsymbol{\omega})dV \\ &-\int_{S_0}\left\{G\cdot\boldsymbol{n}\cdot\frac{\partial \boldsymbol{u}}{\partial t} + \nu\cdot\boldsymbol{n}\cdot(\nabla G\times\boldsymbol{\omega})\right\}dS_0 . \end{aligned} \tag{21}$$

Here, $\beta = 1$ inside the flow volume V and $\beta = 1/2$ on the boundary surface S_0. G is the fundamental solution of the scalar Laplace equation with the delta function expressed as

$$G = \frac{1}{2\pi}\log\left(\frac{1}{R}\right) \tag{22}$$

and H is the Bernoulli-type variable, defined as follows:

$$H_i = \frac{p_i}{\rho} + \frac{u_i^2}{2} . \tag{23}$$

The pressure field of the propulsion mechanism is calculated from the pressure distribution on the body surfaces using Eqs. (21) and (23) during each time step, and with this information, isobaric lines of the entire flow field are computed.

2.4 Calculation of the thrust and drag acting on the wing

The flow force $\mathbf{F}$ acting on the wing of the propulsion mechanism is calculated by integrating the normal component of the pressure p and the tangential component of shear stress τ_w to the wing surface

$$\boldsymbol{F} = \mathbf{i}F_x + \mathbf{j}F_y = \oint_{S_0}\{(-p\cdot\boldsymbol{n}) + \tau_w\cdot\boldsymbol{t}\}dS_0 . \tag{24}$$

Here, F_x and F_y represent the components of force in the x and y directions, respectively, and S_0 represents the integral path according to the wing surface. As shown in the analytical model of Fig. 2, thrust T is the force component in the opposite direction of the uniform flow, which is the direction of the progress of the ship. This value is expressed as $-F_x$ in Eq. (24). Also, drag D is the force component in the direction perpendicular to the uniform flow U, which is a perpendicular component opposite of the wing movement. When the wing moves in the positive direction, it is expressed as $-F_y$, and in the $-y$ direction, it is equivalent to $+F_y$.

The thrust coefficient C_t and the drag coefficient C_d, which shows the dynamic characteristics of the propulsion mechanism, are defined as follows. These definitions are similar to those in the reciprocal type [14, 15]. The circular velocity of the wing shaft $V = r\,\omega$ was set as their representative velocity, and they are given as

$$C_t = \frac{T}{\frac{1}{2}\rho V^2 C} \tag{25}$$

$$C_d = \frac{D}{\frac{1}{2}\rho V^2 C} . \tag{26}$$

Here, r represents the rotation radius, ω is the rotating angular velocity of the wing shaft p with point q as the center as shown in the analytical model of Fig. 2, ρ is the density of the fluid, and C is the wing chord. Also, the propulsive efficiency η is the ratio of the net output generated from the wing to the input and is calculated as follows:

$$\eta = \frac{TU}{\mathbf{M}\bullet\boldsymbol{\omega}}\times 100 . \tag{27}$$

Here, $\mathbf{M}$ represents the torque, and the denominator of Eq. (27), that is, the input, can be calculated as $\mathbf{M}\bullet\boldsymbol{\omega} = \left[F_y\left(x_p - x_q\right) - F_x\left(y_p - y_q\right)\right]\omega$.

3. Results and discussion

First, the conditions for calculation were similar to those in the reciprocal type calculations [13], as done previously. As primary conditions, the uniform flow was set at $U = 1$, the

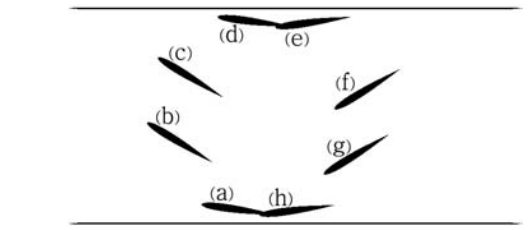

(a) Positions

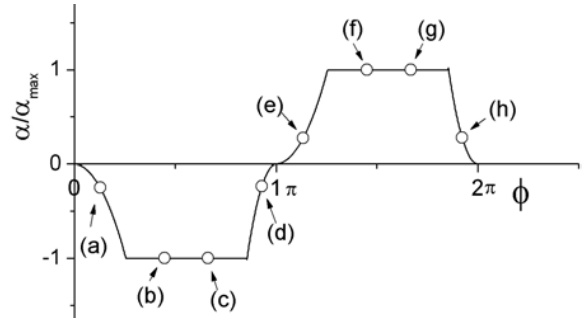

(b) Opening angle

Fig. 5. Positions and opening angle (α) of a wing with the rotating angle (φ) of the rotor for 1 revolution.

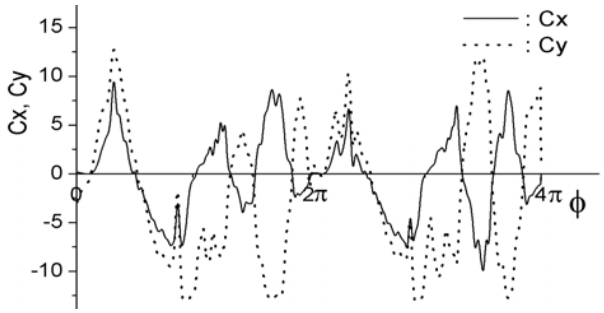

(a) x and y components

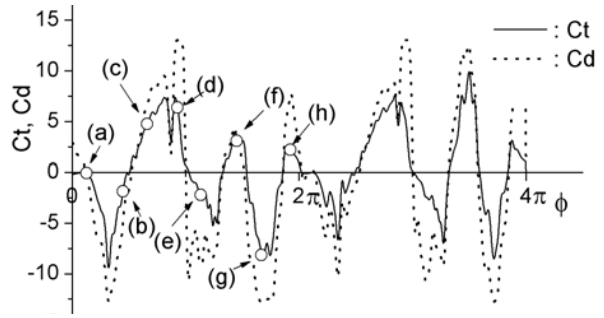

(b) T and D components

Fig. 6. Components of force on the wing with the rotating angle of the rotor (ω = 1.0, (a)-(h) in the figures corresponding to (a)-(h) in Fig. 5).

wing chord was $C = 1$, the rotation radius of the wing shaft was $r = 1.25C$, the maximum opening angle of the wing was $\alpha = 30^\circ$, and the distance from the trailing edge to the wing shaft was $r_a = 0.75C$. The validity of the calculation method such as comparing calculation and experimental results has been sufficiently discussed with the reciprocating type calculations [13].

Fig. 5 shows the changes in the wing position and opening angle α according to the rotating angle ϕ of the wing shaft for 1 revolution. Here, ϕ is the rotating angle from the origin of the wing shaft, that is $\phi = 3\pi/2 - \theta$. In addition, each position (a)-(h) in Fig. 5(a) corresponds to each position (a)-(h) in Fig. 5(b). In other words, (a), (e), (d), and (g) are the middle point of the rotating angle during the opening and closing stages, and (b), (c), (f), and (h) are the points 1/3 and 2/3 into the translating stage. The wing opens from the lower wall with the wing shaft as the center; rotates, maintaining the opening angle α; and finally closes on the upper wall. Then, it repeats the motion: it rotates and opens from the upper wall, moves translationally, and finally rotates and closes on the lower wall.

Fig. 6 shows the force components in the x, y, T, and D directions according to the changes in the rotating angle for 2 revolutions at the angular velocity $\omega = 1.0$. The force coefficients C_x and C_y that acts on the wing in the x and y directions, respectively, and are shown as solid and dotted lines, respectively, in Fig. 6(a), independently fluctuate in the positive (+) and negative (-) directions as the rotating angle ϕ changes. However, in the case of C_t and C_d in Fig. 6(b) in which the force component is divided in the T and D directions, the movement is in the same direction in which the rotating angle ϕ changes, indicating that the dynamic characteristics of the rotating type propulsion mechanism rely heavily on the thrust coefficient C_t and the drag coefficient C_d rather than on the C_x and C_y coefficients. Thus, it is more reasonable to express the characteristics in C_t and C_d. Also, comparing (a)-(h) in Fig. 6(b) with (a)-(h) in Fig. 5 shows that the thrust coefficient started at 0; decreased in the negative direction during the opening stage. Then, during the translational movement, increased in the positive direction; and finally in the closing stage, decreased sharply in the negative direction. In other words, the thrust coefficient strongly fluctuates in both the positive and negative directions when the wing shaft rotates once, and it has 6 inflection points.

Figs. 7 and 8 show the pressure distributions around the wing on the points at which the thrust coefficient had a relatively large positive value and a small negative value. In Figs. 7 and 8, the arrow pointing inward represents the positive pressure, and the arrow pointing outward represents the negative pressure. First, in Fig. 7, to the uniform flow, negative pressure is mostly applied on the pressure face, and positive pressure is applied on the back face. When associated with the opening angle of the wing, this tendency demonstrates that thrust is being applied in the $-U$ direction or the direction of the progress of the ship on the wing in Fig. 2. Contrary to Fig. 7, in Fig. 8, to the uniform flow, positive pressure is mostly applied on the pressure surface, and negative pressure is applied on the back surface. When associated with the opening angle of the wing, this tendency demonstrates that negative thrust is generated in the U direction on the wing in Fig. 2.

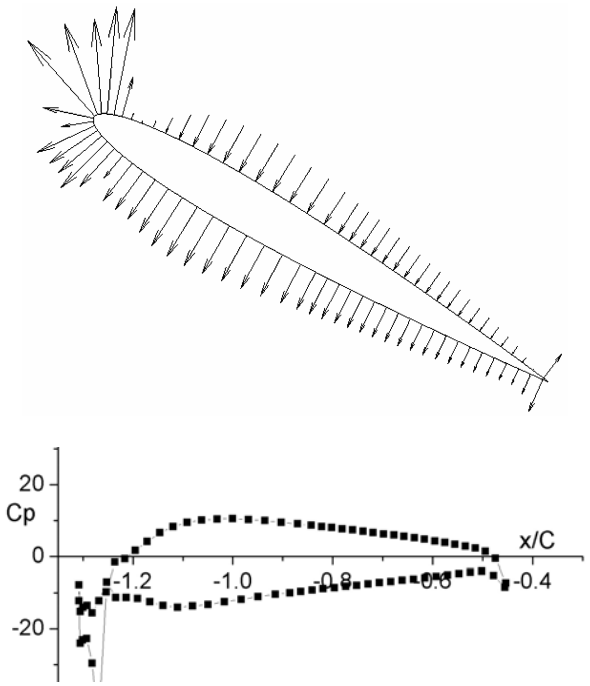

Fig. 7. Pressure distributions around the wing at the (c) point of Fig. 6(b).

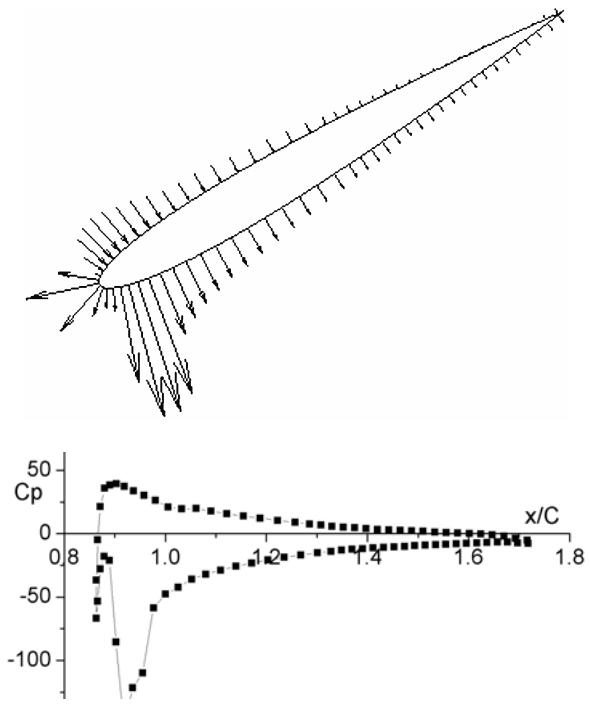

Fig. 8. Pressure distributions around the wing at the (g) point of Fig. 6(b).

Figs. 9 and 10 show the equi-vorticity contour and velocity vectors around the wing in each position for 1 revolution. In Figs. 9 and 10, the points (a)-(h) correspond to those in Fig. 5. For the equi-vorticity of (b) and (c) in Fig. 9, which is the translating stage, separation occurs at the leading and trailing

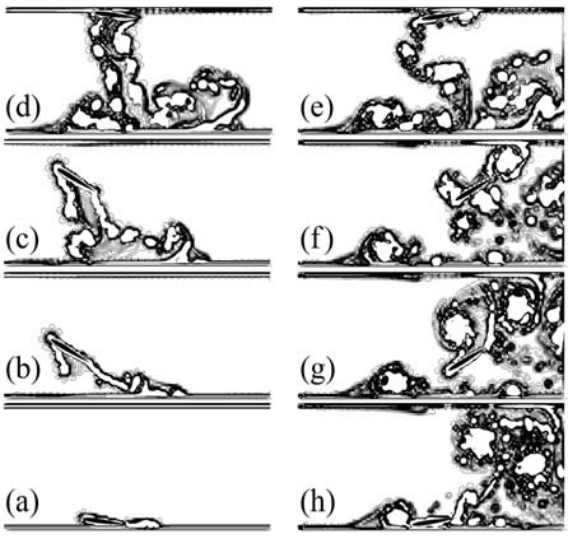

Fig. 9. Equi-vorticity contour around the wing with positions ((a)-(h) in the figure corresponding to (a)-(h) in Fig. 5).

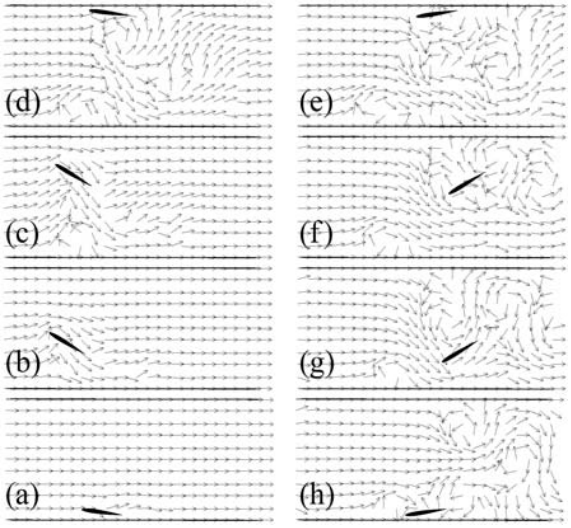

Fig. 10. Velocity vectors around the wing with positions ((a)-(h) in the figure corresponding to (a)-(h) in Fig. 5).

edges of the wing. In the second translating stage of (f) and (g) in Fig. 9, in the early step of this stage, a large vortex is generated around the leading and trailing edges. The vortex is separated from the wing as the wing moves downward and travels to the downstream. When associated with Fig. 8, this tendency demonstrates that in the area around the leading edge, a vortex occurs counterclockwise and in the trailing edge, the vortex occurs clockwise. Also, in (h) of Fig. 9, around the leading edge, a large clockwise vortex is formed. This vortex is due to a separated vortex that is generated from the (b) and (c) stage that was combined with the vortex flow generated from the lower wall of the water channel.

Fig. 11 shows the changes in the thrust coefficient C_t and drag coefficient C_d according to the changes in the rotating angle ϕ in 2 revolutions at the angular velocities ω = 2.0 and

Table 1. Average thrust and drag coefficients and propulsive efficiency with angular velocity.

ω \ Coef.	$\overline{C_t}$ ($\overline{C_t}'$)	$\overline{C_d}$ ($\overline{C_d}'$)	$\bar{\eta}(\%)$
1.0	0.17 (0.27)	-0.69 (-1.08)	2.5
2.0	0.07 (0.44)	-0.33 (-2.06)	27.9
3.0	0.59 (8.30)	0.71 (9.98)	10.0

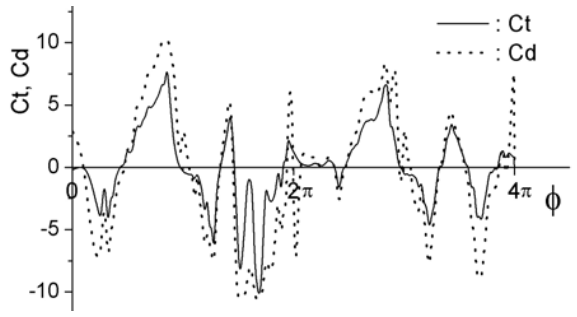

(a) ω = 2.0

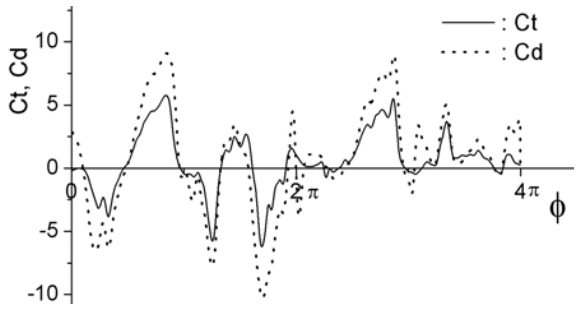

(b) ω = 3.0

Fig. 11. Thrust and drag coefficients on the wing with the rotating angle of the rotor (ω = 2.0, 3.0).

3.0. When Figs. 11(a) and (b) are associated with Fig. 6(b) in this propulsion mechanism, there was almost no change in the qualitative characteristics of the thrust and drag coefficients even though the angular velocity increased. However, when we compared each coefficient in the second revolution, as angular velocity increased, the positive thrust coefficient was larger than the negative coefficient.

Table 1 shows the average propulsive coefficient $\overline{C_t}$, the average drag coefficient $\overline{C_d}$, and the average propulsive efficiency $\bar{\eta}$ according to the changes in the angular velocity. Here, the values of the average thrust and average drag coefficients were an average of the values from Figs. 6(b) and 11(a) and (b). Also, the $\overline{C_t}'$ and $\overline{C_d}'$ values in the parentheses are derived from inserting the uniform flow U in the place of the rotating circular velocity of the wing shaft V in both Eqs. (25) and (26) and then converting them to dimensionless forms. The $\overline{C_t}$ and $\overline{C_d}$ values, converted to dimensionless forms by V^2, showed almost no change when the angular velocity ω increased, but the $\overline{C_t}'$ and $\overline{C_d}'$ values, converted to dimensionless forms by U^2, increased very sharply. The average propulsive efficiency $\bar{\eta}$ was 27.9%, the maximum value, when the angular velocity was $\omega = 2.0$.

4. Conclusions

In this study, we proposed a rotating type propulsion model that applied the principle of the Weis-Fogh mechanism and calculated the unsteady flow field of the propulsion model with the advanced vortex method. The primary condition was set with the uniform flow $U = 1$, the wing chord $C = 1$, the rotation radius of the wing shaft $r = 1.25C$, and the maximum opening angle of the wing $\alpha = 30°$. We investigated the thrust and drag coefficients, pressure field, vorticity field, velocity vector field, and average propulsive efficiency of the propulsion model by changing the rotating angle velocities to $\omega = 1.0$, 2.0, and 3.0. The summary of results is as follows:

(1) The force acting on the wing depended heavily on the directions of the thrust and drag rather than the flow and perpendicular flow directions.

(2) The thrust and drag coefficients strongly fluctuated with the change in the rotating angle of the rotor.

(3) The average thrust increased as the rotating angular velocity increased.

(4) The maximum propulsive efficiency was 27.9% at the angular velocity $\omega = 2.0$.

The flow field of this rotating type propulsion mechanism is unsteady and very complex because the wing rotates and moves unsteadily in the channel. However, using the advanced vortex method, it could be calculated accurately.

Nomenclature

A : Area of vorticity layer element
A_{vor} : Area of nascent vortex element
C : Chord length of wing
C_d : Drag coefficient
C_t : Thrust coefficient
C_p : Pressure coefficient
D : Drag acting on the wing
dt : Time step size
F : Force vector
F_x : X component of the force acting on the wing
F_y : Y component of the force acting on the wing
G : Fundamental solution of scalar Laplace equation
H : Bernoulli-type variable
h : Width of the water channel
h_i : Thickness of vorticity layer at i node of panel
h_{vor} : Thickness of nascent vortex element
i : Unit vector in the x direction
j : Unit vector in the y direction
k : Unit vector in the z direction or the k^{th} time step
M : Rotating moment of the wing or number of panels
M_b : Number of panels for each object
N : Number of vortex elements
N_b : Number of vortex elements from each object

$\mathbf{n}$: Unit normal vector
n_0 : Unit normal vector of a point on boundary surface
$\mathbf{n}_i$: Unit normal vector of i - th control point
p : Center axis of the wing or pressure
q : Rotating axis of the wing
r : Rotating radius of the wing axis
$\mathbf{r}$: Position vector of the rotating radius or position vector of vortex elements
$\mathbf{r}_0$: Position vector of a point on boundary surface
r_a : Distance from the trailing edge of the wing to the wing axis
r_b : Distance from the leading edge of the wing to the wing axis
r_p : Distance from the trailing edge of the wing to the p-point
S_0 : Boundary surface
S_b : Length of each object perimeter
s_i : Panel length at i node panel
T : Thrust acting on the wing
t : Time or non-dimensional time
$\mathbf{t}$: Unit tangential vector
U : Uniform flow
u : $|\mathbf{u}|$
u_i : Tangential velocity at i node of a panel
$\mathbf{u}$: Velocity vector
$\mathbf{u}_i$: Induced velocity at i - th control point
$\mathbf{u}^{sp}$: Induced velocities by source panels
$\mathbf{u}^{vo}$: Induced velocities by vortex elements
$\mathbf{u}^{vp}$: Induced velocities by vortex panels
V : Movement velocity of the wing axis or circular velocity
V_c : Normal convective velocity
V_d : Diffusion velocity at out boundary of vorticity layer
x : X coordinates or x axis
y : Y coordinates or y axis
z : Complex function

Greek letters

α : Opening angle or maximum opening angle
Γ : Circulation involved in vorticity layer element
Γ_b : Circulation of each object circumference
Γ_b^{vo} : Circulation of the vortex element from each object
γ_{bs} : Circulation of unit length for each object circumference
δ : Displacement thickness of vorticity layer
ε_k : Core radio for k - th vortex element
η : Propulsive efficiency
μ : Viscosity coefficient of fluid
ν : Kinematic viscosity of fluid
θ : Rotating angle at complex function
ρ : Density of fluid
τ : Uunit tangential vector
τ_w : Shearing stress on the wall surface
$\mathbf{v}_A$: Velocity vector of any point on the wing
Ω : Rotating angular velocity around the p axis
ω : Rotating angular velocity around the q axis
ω_{vor} : Vorticity of nascent vortex element
$\boldsymbol{\omega}$: Vorticity vector or rotating angular velocity vector
ϕ : Rotating angule from the starting point of the wing

Subscripts

0 : Boundary surface
A : Any point on the wing
b : Object
bs : Object surface
c : Convective
d : Drag or diffusion
p : Point or pressure
q : Point
t : Thrust or trailing edge
vor : Nascent vortex
w : Wall surface
x : X component
y : Y component

Superscripts

sp : Source panels
vo : Vortex elements
vp : Vortex panels
– : Average

References

[1] T. Weis-Fogh,, Quick estimates of flight fitness in hovering animals, Including Novel Mechanism for Lift Production, *Journal of Experimental Biology*, 59 (1973) 169-231.
[2] M. J. Lighthill, On the Weis-Fogh mechanism of lift generation, *Journal of Fluid Mechanics*, 60 (1973) 1-17.
[3] T. Maxworthy, Experiments on the Weis-Fogh mechanism of lift generation by insects in hovering flight, Part 1, Dynamics of the 'Fling', *Journal of Fluid Mechanics*, 63 (1979) 47-63.
[4] R. H. Edwards and H. K. Cheng, The separation vortex in the weisfogh circulation-generation mechanism, *Journal of Fluid Mechanics,* 120 (1982) 463-473.
[5] G. R. Spedding and T. Maxworthy, The generation of circulation and lift in a rigid two-dimensional fling, *Journal of Fluid Mechanics*, 165 (1986) 247-272.
[6] K. D. Ro and M. Tsutahara, Numerical analysis of unsteady flow in the Weis-Fogh mechanism by the 3D discrete vortex method with GRAPE3A, *Journal of Fluids Engineering*, 119 (1997) 96-102.
[7] S. S. Zhang, X. H. Wu and X. F. Wang, Research and progress of Weis-Fogh mechanism hydrodynamics,"*Journal of Hydrodynamics*, 3 (1999) 55-60.
[8] S. B. Furber and Ffowcs Williams, J. E., Is the Weis-Fogh principle exploitable in turbomachinary?, *Journal of Fluid Mechanics*, 94-3 (1979) 519-540.

[9] M. Tsutahara and T. Kimura, An application of the Weis-Fogh mechanism to ship propulsion, *Journal of Fluids Engineering*, 109 (1987) 107-113.
[10] M. Tsutahara and T. Kimura, A pilot pump using the Weis-Fogh mechanism and its characteristics, *Transactions of the Japan Society of Mechanical Engineers*, 54-498 (1988) 393-397.
[11] M. Tsutahara and T. Kimura, Study of a fan using the Weis-Fogh mechanism (An experimental fan and its characteristics), *Transactions of the Japan Society of Mechanical Engineers*, 60-571 (1994) 910-915.
[12] S, S. Zhang, X. H. Wu and X. F. Wang, Hydrodynamic model of Weis-Fogh mechanism hydrofoil, *Journal of Hydrodynamics*, 4 (1996) 35-39.
[13] K. D. Ro, B. S. Zhu and H. K. Kang, Numerical analysis of unsteady viscous flow through a Weis-Fogh type ship propulsion mechanism using the advanced vortex method, *Journal of Fluids Engineering*, 128 (2006) 481-487.
[14] K. D. Ro, Performance improvement of Weis-Fogh type ship's propulsion mechanism using rubber type elastic wing, *Journal of Mechanical Science and Technology*, 23 (3) (2009) 836-844.
[15] K. D. Ro, Performance improvement of Weis-Fogh type ship's propulsion mechanism using a wing restrained by an elastic spring, *Journal of Fluids Engineering*, 132 (4) (2010) 041101-1~041101-6.
[16] K. D. Ro and J. Y. Seok, Sailing characteristics of a model ship of Weis-Fogh type, *Transactions of the Korean Society Mechanical Engineers,* 34 (1) (2010) 45-52.
[17] K. D. Ro, B. K. Choi, J. H. Lee and S. K. Oh, Vibration characteristics of a model ship with Weis-Fogh type ship's propulsion mechanism, *Journal of the Korean Society Marine Engineering*, 34 (1) (2010) 69-75.
[18] K. Kamemoto, On attractive features of the vortex methods, computational fluid dynamics review 1995, ed. M. Hafez and K. Oshima, *Wily&SONS, New York* (1995) 334-353.
[19] A. Leonard, Vortex methods for flow simulations, *Journal of Computational Physics,* 37 (1980) 289-335.
[20] J. S. Uhlman, An integral equation formulation of the equation of motion of an incompressible fluid, *Naval Undersea Warfare Center T.R.* (1992) 10-086.

Ki-Deok Ro received his B.S. degree in Marine Engineering from Pukyong National University, Korea, in 1977. He then received his M.S. and Ph.D degrees from Kobe University, Japan, in 1986 and 1989, respectively. Dr. Ro is currently a Professor at Department of Mechanical Engineering at Gyeongsang National University in Gyeongnam, Korea. He serves as a Vice President of Journal of the Korean Society of Marine Engineering. Dr. Ro's research interests include fluid mechanics, CFD, and vortex method.

BaoshanZhu graduated from the Department of Hydraulic Engineering of Tsinghua University, China, with a bachelor's degree in 1990 and master's degree in 1994, respectively. He then received his doctor's degree from Yakohama National University, Japan, in 1999. Dr. Zhu is currently an associate professor at Department of Thermal Engineering of Tsinghua University, China. His major research interests are fluid mechanics, flow analysis and optimization design for fluid machinery and clean energy.

Michihisa Tsutahara graduated from Department of Aeronautical Engineering of Kyoto University in 1971 and received Ph.D in Applied Mechanics from the University of Michigan in 1982. He was working for Kobe University as a research associate from 1971 to 1986, an associate professor from 1986 to 1992, and a professor from 1992 to 2011. He retired from Kobe University in 2011 and now is a professor emeritus. Dr. Tsutahara's research interests are fluid mechanics, computational fluid dynamics and aerodynamic sounds. He is fellows of Japan Society of Mechanical Engineers and Japan Society of Fluid Mechanics.